European Polymer Journal 112 (2019) 539–546

Contents lists available at ScienceDirect

European Polymer Journal

journal homepage: www.elsevier.com/locate/europolj

Molecular crowding facilitates assembly of spidroin-like proteins through phase separation

Laura Lemetti[a], Sami-Pekka Hirvonen[b], Dmitrii Fedorov[a], Piotr Batys[a,c], Maria Sammalkorpi[a,d], Heikki Tenhu[b], Markus B. Linder[a,*], A. Sesilja Aranko[a,*]

[a] Department of Bioproducts and Biosystems, School of Chemical Engineering, Aalto University, Kemistintie 1, 02150 Espoo, Finland
[b] Department of Chemistry, University of Helsinki, A. I. Virtasen aukio 1, 00014 Helsingin yliopisto, Finland
[c] Jerzy Haber Institute of Catalysis and Surface Chemistry, Polish Academy of Sciences, Niezapominajek 8, PL-30239 Krakow, Poland
[d] Department of Chemistry and Materials Science, School of Chemical Engineering, Aalto University, Kemistintie 1, 02150 Espoo, Finland

ARTICLE INFO

Keywords:
Liquid-liquid phase separation
Coacervation
Self-coacervation
Molecular crowding
Fusion protein
Isothermal titration calorimetry
FRAP
Biopolymer
Spidroin

ABSTRACT

Gaining insights into the processes that transform dispersed biopolymers into well-ordered structures, such as soluble spidroin-proteins to spider silk threads, is essential for attempts to understand their biological function and to mimic their unique properties. One of these processes is liquid-liquid phase separation, which can act as an intermediate step for molecular assembly. We have shown that a self-coacervation step that occurs at a very high protein concentration (> 200 gl^{-1}) is crucial for the fiber assembly of an engineered triblock silk-like molecule. In this study, we demonstrate that the addition of a crowding agent lowers the concentration at which coacervation occurs by almost two orders of magnitude. Coacervates induced by addition of a crowding agent are functional in terms of fiber formation, and the crowding agent appears to affect the process solely by increasing the effective concentration of the protein. Furthermore, induction at lower concentrations allows us to study the thermodynamics of the system, which provides insights into the coacervation mechanism. We suggest that this approach will be valuable for studies of biological coacervating systems in general.

1. Introduction

Liquid-liquid phase separation, also known as coacervation, is a well-known phenomenon for many polyelectrolytes [1]. Liquid-liquid phase separation has been reported to play an important role for biological processes ranging from the formation of proteinaceous membrane-less organelles (PMLOs) [2–5] and spindle assembly [6], to the assembly of underwater adhesives [7,8], amyloid formation [9], and the assembly of biopolymeric materials [10–14]. Coacervation of biopolymers, such as elastin [12] and squid beak proteins [10,11] is reported to have a role in assembling molecules as an intermediate step prior to the final transition from liquid to solid.

Spider silk is an extraordinary example of the properties that a natural fiber can possess. It has high tensile strength yet it is very elastic, both properties leading to extreme toughness that one has so far escaped attempts at synthetic reproduction [15]. In addition, spider silk is biodegradable and causes low immunogenic response which makes it attractive for biomedical applications [16]. On a molecular level, spider silk consists of proteins with long highly repetitive regions capped by globular terminal domains [14,17,18]. Typical to biological materials, the properties of spider silk stem from weak inter- and intramolecular interactions and a precise molecular alignment of the constituent spider silk proteins [19]. Synthetic approaches to producing spider silk-mimicking fibers are attractive, but both the recombinant production of full-length spider silk and the assembly of the fibers have proven challenging [14]. Progress in recombinant DNA technologies allow the production of shorter spider silk-mimicking proteins in bacteria, but the molecular assembly of soluble proteins remains challenging and the biologically relevant mechanisms are at the moment not fully understood.

In a previous study, we described that a silk-like triblock fusion protein self-coacervates in high protein concentration in water, yielding droplets that coalesce spontaneously, relax back to spherical structures after fusing together, and easily wet surfaces. Importantly, coacervation seems to be an important part of the early steps of assembly to various fibrous structures [20]. The coacervation occurred in solutions containing only the triblock fusion protein, and hence the system is classified as a self-coacervating one, as opposed to systems where polymers of at least two types form complexes, leading to complex coacervates [11,21]. The triblock architecture was essential for achieving high

* Corresponding authors.
E-mail addresses: markus.linder@aalto.fi (M.B. Linder), sesilja.aranko@aalto.fi (A.S. Aranko).

https://doi.org/10.1016/j.eurpolymj.2018.10.010
Received 1 September 2018; Received in revised form 8 October 2018; Accepted 9 October 2018
Available online 10 October 2018

solubility and functionality of the coacervates. Native terminal domains were not required, but could be replaced with for example unrelated folded domains such as cellulose-binding modules (CBMs) [22]. The exact nature of the terminal domains was not crucial for function but CBMs proved to function well for high solubility, good production levels, and coacervate formation [20,23].

In this present work, we investigate the coacervation process of the silk-like triblock fusion protein by studying effects of a crowding agent. Crowding agents have previously been used to study compartments in nuclei [24,25], protein folding [26,27], spindles [6], and non-membrane-bound organelles [4] *in vitro*. Crowding effects arise from a combination of excluded volume and either increased attractive or repulsive interactions between molecules [28]. Molecular crowding has also been noticed to promote amyloid formation and therefore for example the incidence of neurogenerative diseases [9]. Despite the fact that the local concentration of a given protein is often low inside cells, the overall macromolecule concentration can reach hundreds of grams per liter, making the cellular environment highly crowded [28,29].

Our aim in this study was to obtain deeper understanding of the process of coacervation of silk like proteins, as we have found in previous studies that coacervation is a key intermediate step in their functional assembly into fibers. In this study, we demonstrate that crowding agents lead to concentration-dependent coacervation of an engineered triblock silk-like fusion protein CBM-eADF3-CBM [20], which consists of a repeat region mimicking silk sequence capped by two globular domains (Fig. 1). We study the mechanism, by which the crowding agent affects the coacervation, and show that it does not interact with the protein. Finally, we investigate the thermodynamics of the system. By exploring the conditions leading to coacervation and developing systematic methods to study coacervation, we aim at developing an understanding that will lead to new ways to apply these biopolymers as sustainable and highly functional materials.

2. Experimental section

2.1. Fusion protein

The fusion protein studied in our work has a triblock structure (Fig. 1). An engineered version (eADF3) [30] of the ADF3 dragline sequence [31] from *Araneus diadematus* was used as the middle block. It is a highly repetitive sequence consisting of 12 consecutive A- and Q-rich blocks. Globular terminal groups, cellulose-binding modules (CBM) [22] from *Clostridium thermocellum* cellulosome, were fused to the middle block with 2 kDa linkers. We refer to this protein as a triblock spidroin-like protein in this report and use abbreviation CBM-eADF3-CBM for it. The molecular weight of CBM-eADF3-CBM is 85 kDa, the CBM terminal units being 17 kDa each and the silk sequence in the middle 46 kDa. A C-terminal his-tag was added for affinity purification. The cloning of CBM-eADF3-CBM and CBM, which is used as a control, has been described earlier [20].

Recombinant silk proteins CBM-eADF3-CBM and the terminal group CBM alone were produced in *Escherichia coli* strain BL 21(DE3) using Magic Media *E. coli* expression medium (Thermo Fisher Scientific) according to the manufacturer's protocol. Purification after lysis was carried out by precipitating other *E. coli* proteins by heating at 70 °C for 30 min followed by buffer exchange with Econo-Pac 10 DG desalting columns (Bio-Rad). This was sufficient to remove the majority of impurities from the sample.

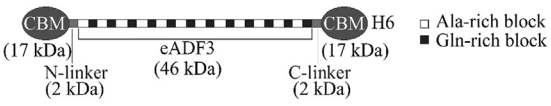

Fig. 1. Schematic structure of the CBM-eADF3-CBM triblock fusion protein which consists of 12 repeating A- and Q-rich blocks (eADF3) fused with globular terminal groups (CBM) via linkers.

2.2. Labelled CBM-eADF3-CBM

To label CBM-eADF3-CBM, Oregon Green 488 carboxylic acid succinimidyl ester (Thermo Fisher Scientific) was dissolved in dimethylformamide (DMF, Fisher Scientific) at 10 gl^{-1} and added to the protein solution that had been adjusted to pH 8.5 by addition of 1 M $NaHCO_3$. The reaction was carried out at room temperature for one hour and protected from light. Unreacted dye was removed immediately using Econo-Pac 10DG desalting columns (Bio-Rad). The labeled protein was concentrated to the desired concentration using a Vivaspin 20 centrifugal concentrator (30 kDa cut-off) (Sigma Aldrich).

2.3. Instrumental methods

2.3.1. Optical and fluorescence microscopy

Axio Vert.A1 and Observer.Z1 inverted optical microscopes (Carl Zeiss, Germany) were used to image phase-separated samples. The Observer was equipped with a motorized stage and either AxioCam MRm or Andor iXon Ultra 888 camera whereas Axio Vert.A1 was equipped with AxioCam 503 color camera.

In order to image the distribution of Oregon Green labeled dextran (70 kDa) in the sample, brightfield and fluorescent images were acquired using an Andor iXon Ultra 888 camera. Images were captured with a 1.6 optovar using either a 20×/0.5 Phase contrast or 100×/1.3 Phase contrast oil objective. Fluorescent signal was obtained using excitation light at 470 nm, while collecting the emitted light of 461–485 nm.

Protein and dextran samples were prepared beforehand in several different concentrations in water and prior to measurement mixed in 1:1 ratio in order to reach the final concentrations. For labeling studies, Oregon Green labeled dextran (80 gl^{-1}, 70 kDa) was mixed with a solution of unlabeled dextran (80 gl^{-1}, 500 kDa) in 1:1 ratio. This mixture was then mixed with the protein in 1:1 ratio. Imaging was always done without a cover glass in order not to distort the actual structure and movement of the coacervates.

2.3.2. Scanning Electron Microscopy (SEM)

Electron microscopy imaging was carried out at the Nanomicroscopy Center at Aalto University with Zeiss Sigma FE-SEM with variable pressure. A secondary electron detector and 1.5 kV EHT was used. Samples were coated with 7 nm of Platinum or Platinum/Palladium.

2.3.3. Sedimentation experiments with Analytical Ultracentrifuge (AUC)

Sedimentation velocity experiments were performed with an Optima Analytical Ultracentrifuge (AUC) (Beckman Coulter) to study the possible interaction between the terminal group CBM and dextran. Both samples were measured separately at a concentration of 0.4 gl^{-1}. A mixture of dextran and CBM in 1:1 ratio was also studied. 20 mM NaCl was used in all samples to prevent electrostatic interactions. Sedimentation experiments for dextran were performed using interference detection at 42 000 rpm. CBM and the mixture of CBM and dextran were measured by UV absorbance at 280 nm at 50 000 rpm. The temperature during all experiment was 20 °C. All samples were allowed to achieve temperature equilibrium in the centrifuge chamber for 90 min prior to starting the experiment.

AUC data were analyzed using Ultrascan version 4.0 revision 2528 (http://www.ultrascan.uthscsa.edu) [32]. The partial specific volume of CBM was calculated to be 0.7148 from its amino-acid sequence [33]. Time-invariant and radial-invariant noises were removed by 2D spectrum analysis (2DSA) [34]. Regularization of the 2DSA results and determination of size distributions were performed by Monte Carlo analysis [35].

2.3.4. Fluorescence Recovery after Photobleaching (FRAP)

Fluorescence Recovery after Photobleaching (FRAP) was used to

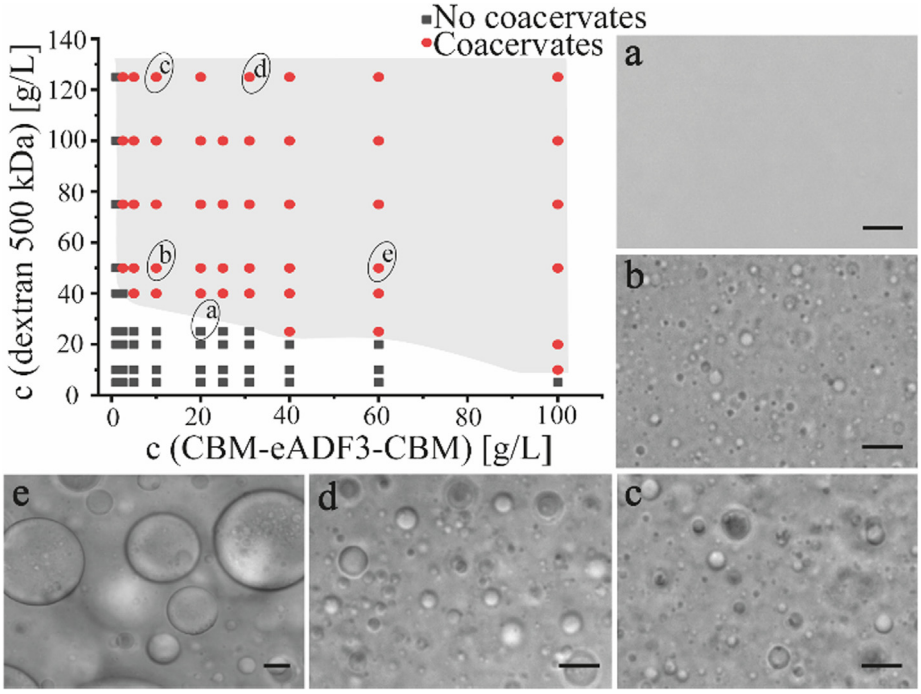

Fig. 2. Phase diagram of the triblock spidroin-like protein CBM-eADF3-CBM with dextran (500 kDa). The gray area shows roughly the area where the CBM-eADF3-CBM is phase separated. Pictures taken with a light microscope show the coacervates at different regions of the phase diagram. Scale bar 10 μm.

measure the diffusion of a fluorescently labeled protein [36]. A small area of fluorescent sample (2–5 μm) was photobleached with a focused laser beam and following the recovery of the lost fluorescence was monitored.

FRAP imaging was carried out at Light Microscopy Unit, Institute of Biotechnology. Data were recorded with Leica TSC SP5 confocal microscope with FRAP booster using 63× 1.2NA water objective. Argon laser (488 nm) and a 488/561 dichroic beam splitter were used. Data were analyzed with the Leica AF Lite – TCS MP5 software and further processing was carried out in Matlab. Fitting was carried out according to Eq. (1) [36]

$$D = (V_0^2\gamma_D/4\gamma_F^2)[(\tau_{1/2}^C)^2/\tau_{1/2}] \quad (1)$$

where V_0 is the known velocity of the calibration scan, $\tau_{1/2}$ and $\tau_{1/2}^C$ represent the 50% recovery times for the diffusion experiment and the calibration scan, and γ_D and γ_F are functions of the beam shape and the extent of bleaching.

2.3.5. Fourier Transform Infrared Spectroscopy (FTIR)

Perkin Elmer Spectrum 2 FTIR with ATR spectrometer was used to record FTIR. All spectra were scanned over the range 400–4000 cm^{-1} with 4 scans and a resolution of 32 cm^{-1}. Sample solvents (H_2O) were exchanged to D_2O using Vivaspin 6 centrifugal concentrators (30 kDa cut-off) prior to measurement.

2.3.6. Determination of critical overlap concentration c* of dextrans

The viscosities of dextran solutions were determined using Discovery HR-2 hybrid rheometer (TA Instruments) equipped with Peltier thermostatic plate at 20.0 °C. The geometry used was plate and cone with 60 mm 1.999° stainless steel cone having tip truncation of 62 μm. The sample volume used was 1.92 ml. Measurements were performed as shear sweeps varying the shear rate between 1 and 1000 s^{-1} with 5 points per decade and with a maximum of 60 s to achieve steady state flow after which the value was recorded if steady state was not established. The Newtonian flow range was found to be 10–100 s^{-1} and values recorded at 25 s^{-1} were used in calculations. Extrapolated zero-shear viscosity was not used because difficulties in performing a proper fit to data recorded at lower concentrations. Samples were prepared by dissolving dextran overnight in water in volumetric flask to make a stock solution at 120 gl^{-1}. The stock solution was then used to make the solutions for rheology measurements by dilution with water

2.3.7. Isothermal Titration Calorimetry (ITC)

ITC measurements were performed on a VP-ITC Microcalorimeter (MicroCal, Northampton, USA). All measurements were performed in constant sodium chloride (NaCl, 20 mM). Protein samples were exchanged from water to 20 mM NaCl solution gradually in a Vivaspin 20 centrifugal concentrator (30 kDa cut-off) by washing the protein solution four times with a 20 mM NaCl solution. Samples were then concentrated to the desired value with these same concentrators. Samples were degassed under vacuum with mixing for 15 min always prior to the measurement.

Experiments were carried out at 25 °C and with 45 injections, each with a volume of 2 μl. The spacing between injections was 300 s to ensure that the system had returned to equilibrium. The stirring speed was 307 rpm. The reference cell was filled with degassed water and the sample cell either 20 mM NaCl or 60 gl^{-1} dextran (500 kDa) in 20 mM NaCl. All measurements were performed in triplicates.

3. Results and discussion

The liquid-liquid phase separation of CBM-eADF3-CBM occurred at protein concentrations above 200 gl^{-1} with water acting as the solvent. To study the effect of a crowding agent on the phase separation dextran, a slightly branched polysaccharide was used [37], as it is reported to lack attractive interactions with proteins [38]. Dextran has been used widely in food and biomedical industry [39] and also as a crowding agent when studying the compartments within the nucleus [24,25]. By adding dextran (500 kDa) at different concentrations we found that phase separation occurred at much lower protein concentrations (Fig. 2). At dextran concentrations at around 10 gl^{-1} the phase separation occurred at protein concentrations around 100 gl^{-1}. At higher dextran concentrations, with a marked change around 50 gl^{-1} dextran,

phase separation occurred already at protein concentrations of 2.5 gl^{-1}. We observed similar effects when using dextran of different molecular weights (20, 70, and 110 kDa) or Ficoll, another commonly used and relatively inert crowding agent, which indicated that the results may apply to crowding agents in general (data not shown).

The size distribution of the coacervate droplets was broad and coacervates gained size by spontaneous coalescence (Supplementary information Fig. 1). The coacervate droplets had the same round shape whether they were induced by raising the concentration of protein or through the addition of dextran. Based on optical microscopy and the behavior of coacervates we noted that the addition of dextran led to phase separation that was indistinguishable from the system without added dextran.

The phase diagram showing the coacervating conditions were highly reproducible. Conditions near the phase border resulted consistently in the same phase behavior. In Fig. 2, light microscope images show that the coacervate droplets had slightly different appearance in different regions of the diagram, with the droplet size increasing in both the direction of protein and dextran concentrations, but overall the largest droplets occurred at the highest protein concentrations.

To understand the clear and reproducible effect of dextran on coacervation, we explored two hypotheses further; one being that dextran acts as a crowding agent and by excluded-volume effects increases the effective concentration of the silk-like biopolymer and thereby to form coacervates, and the other that dextran interacts with the silk-like biopolymer to create complexes leading to complex coacervates.

To investigate a possible interaction between the CBM and the dextran, we analyzed the effect of dextran on the sedimentation of CBM by AUC. Samples were analyzed either by interferometry (660 nm) that shows all molecular components of the sample or by UV absorption that only identifies the CBM (280 nm), even in a mixed sample. The sample containing pure dextran displayed a wide distribution of peaks, due to the heterogeneity of the sample, which complicated the analysis (Fig. 3a). Data are plotted on a pseudo 3D plot in which partial concentration, sedimentation coefficient (S), and frictional ratio (f/f0) are displayed. In the sample containing mixture of dextran and CBM a clearly identifiable peak of CBM with the sedimentation coefficient of about $2.15*10^{-13}$ and the frictional ratio 1.2 showed up (Fig. 3b). The faint peaks around the main peak were identified as stochastic noise in the fitting and were not considered further. A control sample of pure CBM displayed a peak for CBM identical to that in the pure sample (data not shown). No shift or increased distribution in values of S and f/f0 was observed between the samples containing CBM and the mixture of CBM and dextran indicating no interaction between them.

To further exclude the possibility of complex coacervation, we investigated the distribution of dextran and the silk-like protein in the sample by imaging samples with either CBM-eADF3-CBM or dextran labeled with Oregon Green 488. As seen in Fig. 4, CBM-ADF3-CBM is concentrated inside the droplets (Fig. 4a and b) whereas dextran is excluded from those (Fig. 4c and d). These data show that the dextran is excluded from the coacervates and that the silk-like fusion protein is indeed highly concentrated inside the coacervates.

In our previous studies we have found that one of the most significant properties of the CBM-eADF3-CBM coacervates is that fibers can be pulled directly by extending a droplet of a solution containing these (Fig. 5). If coacervate droplets were not present in the solution it was not possible to draw fibers from the solution. Another characteristic feature of the coacervate droplets is that if these are dried on a surface, and the resulting film is teared, then fibers will form that bridge the cracks. The formation of the extended fibers over the cracks is similar to the effect known as necking in polymers [40] and suggest a semi-crystalline internal structure (Fig. 5b).

Our results show that the functions of fiber drawing and necking remain the same regardless of the presence of dextran. However, the necking in films appeared different in samples with and without dextran (Fig. 5b and e). While necking occurred only in the clearly identifiable drops in the samples without dextran, the samples with dextran showed a more uniform structure and necking occurred throughout the sample. This is likely due to the structural changes in the sample while it dries. During drying both the dextran and protein concentrations increase which may lead to changes in the protein distribution in the sample and a more uniform behavior.

Having established that dextran does not disrupt the functional property of the triblock spidroin protein to form fibers, we continued to study if any differences could be found in the properties of the liquid coacervate droplets. For finding possible differences we used FRAP to measure the diffusion of proteins within coacervate droplets (Fig. 6). For FRAP we used Oregon Green to label CBM-eADF3-CBM and studied it in conditions containing dextran and without dextran. We obtained values for the diffusion constant D of 0.044 $*10^{7}\,cm^{2}\,s^{-1}$ ± 0.005 for coacervates in water and 0.053 $*10^{7}\,cm^{2}\,s^{-1}$ ± 0.011 for coacervates in dextran, showing within the error limits that there are no significant differences between the samples. As the protein diffuses with the same rate regardless of dextran being present in the sample, we conclude that this indicates no direct molecular interaction between these polymers in the coacervates. The non-coacervated CBM-eADF3-CBM had a D of 1.18 $*10^{7}\,cm^{2}\,s^{-1}$ ± 0.078.

We studied effects of the dextran on protein conformation by FTIR.

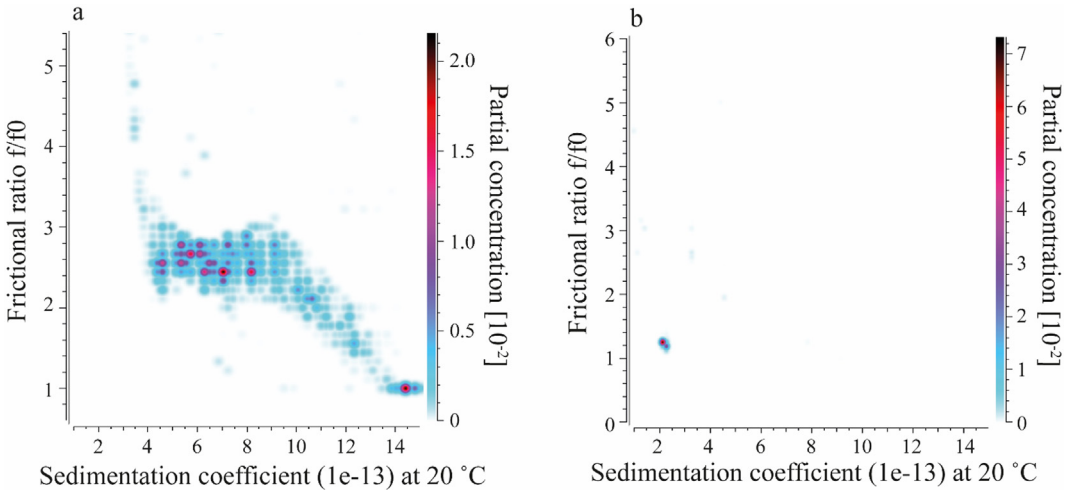

Fig. 3. (a) Pseudo 3D plot of pure dextran measured at 660 nm displaying a wide distribution of dextran with higher f/f0 and S values. (b) Pseudo 3D plot of CBM-dextran mixture measured at 280 nm. A CBM peak is observed at $S = 2.15*10^{-13}$, f/f0 = 1.2. Dextran is invisible at 280 nm. However, in the case of interaction between CBM and dextran, the latter would cause changes in the distribution of CBM.

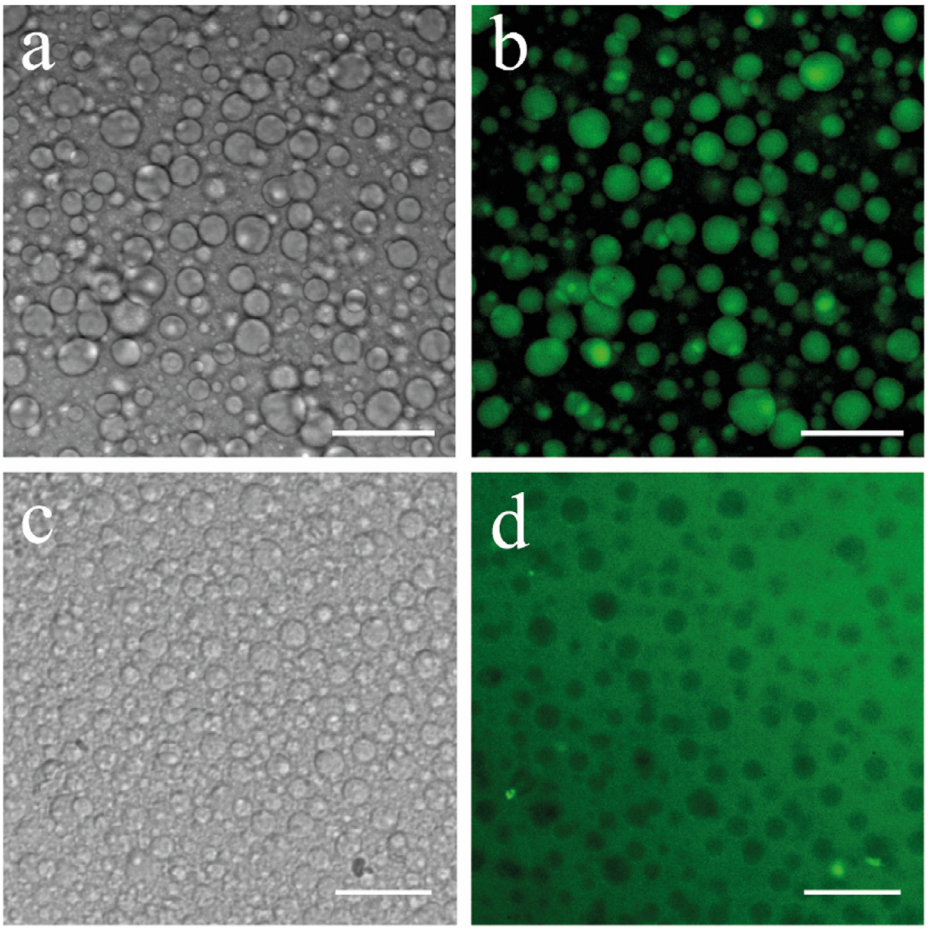

Fig. 4. Images (a) and (b) present the labeled CBM-eADF3-CBM mixed with dextran whereas (c) and (d) present labeled dextran mixed with CBM-eADF3-CBM. Scale bar 50 μm. Dextran concentration 4 gl^{-1} in both.

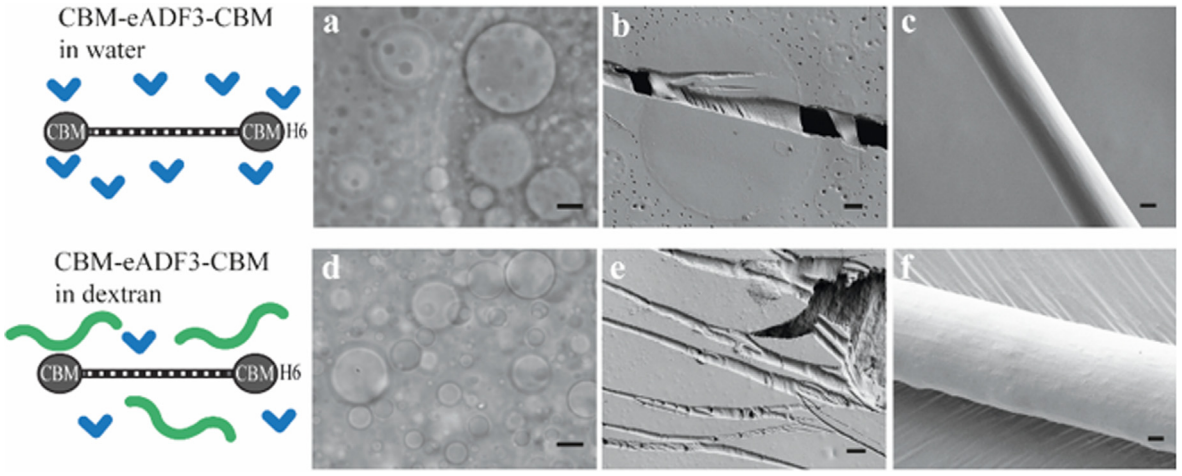

Fig. 5. Optical microscope images of (a) CBM-eADF3-CBM in water, (d) CBM-eADF3-CBM with 3% dextran (500 kDa). Scale bar 10 μm. SEM images (b, e) of the necking as a result of mechanical stretching in a semi-dry state. SEM images of fibers pulled from CBM-eADF3-CBM solutions (c, f). The scale bar in the SEM images 2 μm.

From previous studies it is known that CBM-eADF3-CBM can take different conformations, and that the one present in the coacervates obtained in low salt are high in alpha helices and that addition of phosphate or solvents such as ethanol give additional FTIR signals indicating beta sheet structures [20]. The spectra of samples with and without dextran indicated very similar conformations. The measurement was done in D_2O to minimize the disturbance that H_2O gives to the Amide I band (Fig. 7). It is pointed out that using D_2O as a solvent results in a shift of the Amide II band compared to samples in H_2O [41].

The viscosity of aqueous dextran solutions in a concentration range of 120–4 gl^{-1} was determined in order to calculate the critical overlap concentration c* and to get a good estimate for the transition from dilute solution where individual dextran molecules are able to move relatively freely to semi dilute solution where the swollen coils are in

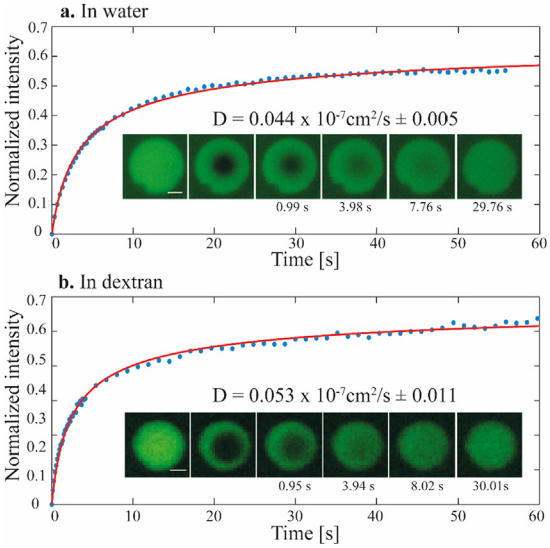

Fig. 6. FRAP recovery of partially bleached CBM-eDAF3-CBM coacervate (a) in water, scale bar 2 μm, and (b) in 10% dextran, scale bar 4 μm. The time scale of images is in seconds after the bleach. Diffusion is presented as a mean value ± std (n = 5).

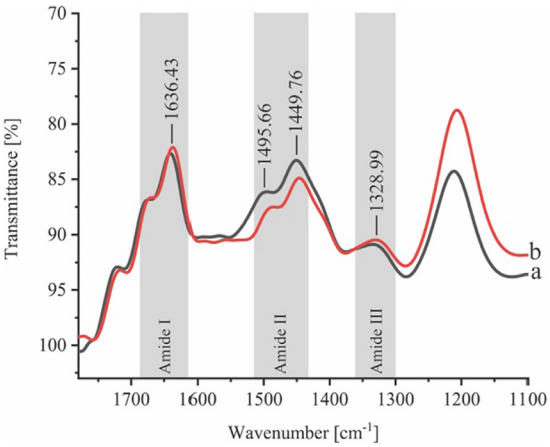

Fig. 7. FTIR spectra of CBM-eADF3-CBM in D_2O (a) and in the presence of 50 gl^{-1} dextran (b). The spectra indicate that there are no significant conformational differences between the protein in the samples.

constant contact with neighboring coils. The value for c* was approximated using the reciprocal of intrinsic viscosity [η]. Intrinsic viscosity was calculated using the viscosity data recorded in the region of 14–4 gl^{-1} thought to be in the dilute region and the specific viscosity values ranging from 0.96 to 0.26. Some concentrations lower than 4 gl^{-1} were also studied but their viscosity was too low for the experimental setup to produce reliable data. The viscosity of water was recorded as solvent viscosity η_0. Intrinsic viscosity was calculated by using the combined method of Huggins and Kraemer. In the double extrapolation Huggins plot (specific viscosity η_{sp}) / concentration vs. concentration) [42] and Kraemer plot ($\ln(\eta_{srel})$/ concentration vs. concentration) [42], the data were extrapolated to zero concentration (Fig. 8). The two sets have equal values at zero concentration and was determined to be 16 gl^{-1}. The values are higher than previously reported (4.6 gl^{-1}) using the same approach [43] but the difference is likely to be attributed to differences production batches the material. Comparing to the phase diagram (Fig. 2) we note that the region in which the dextran starts to have a significant effect on the coacervation is around the c*, where the system is expected to be heavily crowded. Also, it is expected that around dextran there is a several layers of

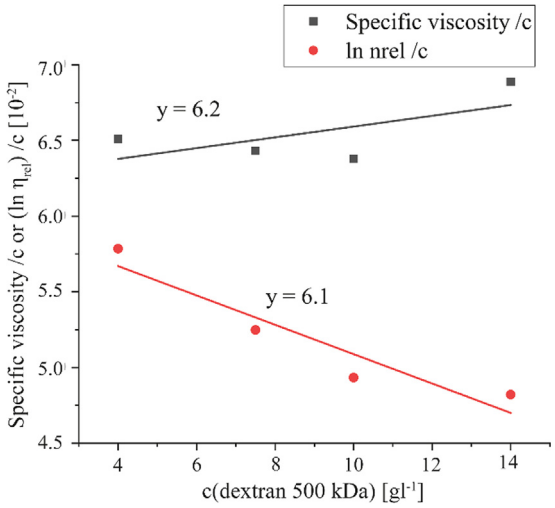

Fig. 8. Huggins (η_{sp}/c vs. c) and Kraemer (($\ln \eta_{rel}$)/c vs. c) plot of dextran 500 kDa.

hydrating water molecules, bound via hydrogen bonds [44]. Therefore, even at relatively low concentration of dextran, the amount of a free water (unaffected by dextran) might be small, and thus the effective concentration of the protein increases, facilitating their assembly.

ITC was used to determine the thermodynamics of the coacervation process with crowding agents. Previously ITC has been mostly used to understand complex coacervation between oppositely charged macromolecules [45] with only very limited results on self-coacervation [11]. In the ITC experiments we added concentrated protein solution to a solution containing dextran, and recorded the heat generated or absorbed at constant temperature [46]. Control experiments included adding protein to buffer and using the CBM instead of CBM-eADF3-CBM as the protein sample solution.

Experiments showed that both protein to buffer and protein to dextran resulted in measurable heats. To avoid heats coming from ion release from the protein, all samples were dialyzed against 20 mM NaCl, which was also used as the buffer solution. Fig. 9 shows the normalized heat change per injection. After each experiment the solutions were inspected by microscopy to verify coacervation. In the samples with CBM-eADF3-CBM added to dextran coacervates were always observed, and in the other samples coacervates were never observed. From experiments halted mid-way and analyzed, we conclude that coacervates formed already before injectant concentrations of 0.3 μM (Fig. 9e). The shape of the raw data (Supplementary information, Fig. 2) shows dual peaks and inflection points from exothermic to endothermic. Magnifications of peak shapes are included in the Supplementary information (Fig. 2). According to other references, such behavior is affiliated to complex formation or coacervation [47].

Protein to buffer measurements were subtracted from protein to dextran measurements in order to achieve the final heat change per injection (Fig. 9g). Measurements were conducted in the same molar concentration of CBMs. After the control reduction we note that both reactions are exothermic, as the heat of injection is negative for both CBM-eADF3-CBM and CBM (Fig. 9g). It has been reported that complex coacervation involving the interaction of two polymers usually is exothermic [48]. However, previously Cai et al. [11] reported that the self-coacervation of histidine-rich beak proteins is much more strongly endothermic. In that case, however, the coacervation was induced by high salt concentrations possibly leading to heat from ion solvation effects. In the present study, we were able to use an identical buffer in all samples, and thereby to minimize such effects.

The data obtained in the ITC experiments did not allow a general binding model to be used for data fitting, due to the complexity of the data. However, a visual comparison between the coacervating sample

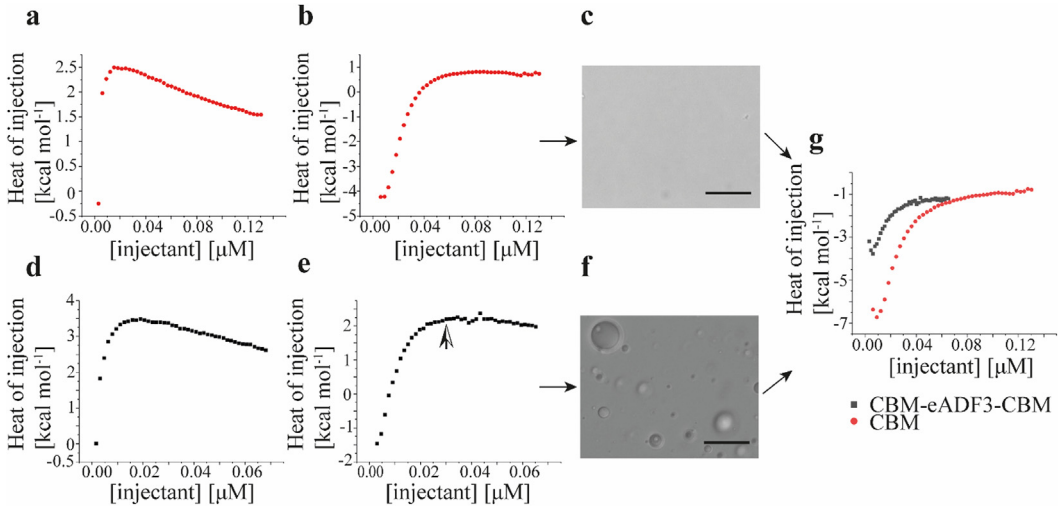

Fig. 9. ITC titration of CBM to water (a) and 6% dextran (b) and CBM-eADF3-CBM to water (d) and 6% dextran (e). Black and white arrow in image (d) shows the point in which the sample has already coacervated. Optical microscope images (c,f) after the measurement. The final isotherms after subtracting protein to water measurements from protein to dextran measurements are shown in (g). Scale bar 20 μm.

and the non-coacervating control lacking the repetitive spidroin sequence (Fig. 9g) allows some conclusions. The difference in the heat per injection for these samples is slightly positive but close to zero. As we know by direct observation that coacervates in fact are formed in the CBM-eADF3-CBM sample, we then conclude that the heat associated with coacervation must be close to zero. That is ΔH = 0 in the equation $\Delta G = \Delta H - T\Delta S$ where ΔG is the change in free energy, ΔH is the change in enthalpy, ΔS is the change in entropy, and T is the temperature. This implies that the coacervation event is driven by changes in entropy, i.e. $\Delta G = -T\Delta S$. To estimate the magnitude of the change in entropy we can use a previous estimation of the concentration difference of CBM-eADF3-CBM inside coacervates and in the dilute solution outside [23]. As the ratio was 140, we obtain a ΔG of $-11\,\mathrm{kJmol^{-1}}$ ($-2.6\,\mathrm{kcalmol^{-1}}$), giving the entropy of coacervation of about $40\,\mathrm{JK^{-1}\,mol^{-1}}$ at 293 K. That the coacervation is entropy-driven fits well with previous suggestions that helix packing and weak protein interactions are responsible for coacervation [20].

4. Conclusions

We have found that dextran functions to lower the protein concentration needed for self-coacervation of a triblock spidroin-inspired protein by a crowding mechanism. There is no interaction between dextran and the protein as analyzed by FRAP and AUC, and the dextran does not affect the properties of the coacervates. The setup allowed thermodynamic studies by ITC that would not be feasible by our previously available methods for achieving coacervation by concentration increase. Based on these observations, we propose an overall mechanism for the coacervation and role of dextran. When the proteins associate, their motion become restricted, as indicated by the drastic drop in the diffusion coefficient. This causes the decrease of their translation entropy. However, at the same time, the water bound to the proteins is being released, increasing the entropy of the system. When the increase in the entropy of water molecule release is larger than the decrease in entropy due to the limited motion of the proteins, coacervation occurs. While this reasoning captures the qualitative origins of coacervation in this system, the underlying molecular interactions remain to be uncovered. These could include contributions from attractive interactions between hydrophobic Ala-stretches or the terminal domains.

The work highlights not only that coacervation can be aided by utilizing crowding agents but also that crowing agents may enable enhanced access to studying the mechanism of coacervation. The finding has potential benefits in processes for future biopolymer-based materials, and for understanding the general mechanisms in biomolecular assembly to form cellular structures and biopolymer assemblies.

Acknowledgements

The work was performed within the Academy of Finland Center of Excellence Programme (20142019) and Academy of Finland projects 307474, and 308772. Authors wish to acknowledge the assistance and support of Marko Crivaro and Mika Molin of the Light Microscopy Unit, Institute of Biotechnology for performing FRAP measurements. We also acknowledge the provision of facilities and technical support by OtaNano – Nanomicroscopy Center (Aalto-NMC). We would also like to thank Christopher Jonkergouw for helping with the imaging of fluorescent dextran, Professor Lasse Murtomaa for providing the ITC equipment and Professor Francoise Winnik for insightful comments of ITC data.

Conflicts of interest

The authors declare no competing interests.

Data availability

The raw/processed data required to reproduce these findings cannot be shared at this time due to technical or time limitations

Appendix A. Supplementary material

Supplementary data to this article can be found online at https://doi.org/10.1016/j.eurpolymj.2018.10.010.

References

[1] C.G. De Kruif, F. Weinbreck, R. De Vries, Complex coacervation of proteins and anionic polysaccharides, Curr. Opin. Colloid Interf. Sci. 9 (2004) 340–349, https://doi.org/10.1016/j.cocis.2004.09.006.
[2] C.P. Brangwynne, Germline P granules are liquid droplets that localize by controlled dissolution/condensation, Science 5 (2009).
[3] C.P. Brangwynne, T.J. Mitchison, A.A. Hyman, Active liquid-like behavior of nucleoli determines their size and shape in Xenopus laevis oocytes, Proc. Natl. Acad. Sci. 108 (2011) 4334–4339, https://doi.org/10.1073/pnas.1017150108.
[4] Y. Lin, D.S.W. Protter, M.K. Rosen, R. Parker, Formation and maturation of phase-separated liquid droplets by RNA-binding proteins, Mol. Cell. 60 (2015) 208–219, https://doi.org/10.1016/j.molcel.2015.08.018.

[5] Y. Shin, C.P. Brangwynne, Liquid phase condensation in cell physiology and disease, Science. 357 (2017), https://doi.org/10.1126/science.aaf4382 eaaf4382.
[6] H. Jiang, S. Wang, Y. Huang, X. He, H. Cui, X. Zhu, Y. Zheng, Phase transition of spindle-associated protein regulate spindle apparatus assembly, Cell 163 (2015) 108–122, https://doi.org/10.1016/j.cell.2015.08.010.
[7] J.H. Waite, Mussel adhesion – essential footwork, J. Exp. Biol. 220 (2017) 517–530, https://doi.org/10.1242/jeb.134056.
[8] R.J. Stewart, C.S. Wang, H. Shao, Complex coacervates as a foundation for synthetic underwater adhesives, Adv. Colloid Interf. Sci. 167 (2011) 85–93, https://doi.org/10.1016/j.cis.2010.10.009.
[9] S. Ambadipudi, J. Biernat, D. Riedel, E. Mandelkow, M. Zweckstetter, Liquid-liquid phase separation of the microtubule-binding repeats of the Alzheimer-related protein Tau, Nat. Commun. 8 (2017) 1–13, https://doi.org/10.1038/s41467-017-00480-0.
[10] Y. Tan, S. Hoon, P.A. Guerette, W. Wei, A. Ghadban, C. Hao, A. Miserez, J.H. Waite, Infiltration of chitin by protein coacervates defines the squid beak mechanical gradient, Nat. Chem. Biol. 11 (2015) 488–495, https://doi.org/10.1038/nchembio.1833.
[11] H. Cai, B. Gabryelczyk, M.S.S. Manimekalai, G. Grüber, S. Salentinig, A. Miserez, Self-coacervation of modular squid beak proteins – a comparative study, Soft Matter. 13 (2017) 7740–7752 http://xlink.rsc.org/?DOI=C7SM01352C.
[12] G.C. Yeo, F.W. Keeley, A.S. Weiss, Coacervation of tropoelastin, Adv. Colloid Interf. Sci. 167 (2011) 94–103, https://doi.org/10.1016/j.cis.2010.10.003.
[13] L.D. Muiznieks, J.T. Cirulis, A. van der Horst, D.P. Reinhardt, G.J.L. Wuite, R. Pomès, F.W. Keeley, Modulated growth, stability and interactions of liquid-like coacervate assemblies of elastin, Matrix Biol. 36 (2014) 39–50, https://doi.org/10.1016/j.matbio.2014.03.008.
[14] M. Heim, D. Keerl, T. Scheibel, Spider silk: From soluble protein to extraordinary fiber, Angew. Chemie - Int. Ed. 48 (2009) 3584–3596, https://doi.org/10.1002/anie.200803341.
[15] A.M. Anton, A. Heidebrecht, N. Mahmood, M. Beiner, T. Scheibel, F. Kremer, Foundation of the outstanding toughness in biomimetic & natural spider silk, Biomacromolecules (2017), https://doi.org/10.1021/acs.biomac.7b00990 acs.biomac.7b00990.
[16] M. Widhe, J. Johansson, M. Hedhammar, A. Rising, Current progress and limitations of spider silk for biomedical applications, Biopolymers. 97 (2011) 468–478, https://doi.org/10.1002/bip.21715.
[17] M. Xu, R.V. Lewis, Structure of a protein superfiber : spider dragline silk J |, Proc. Natl. Acad. Sci. United States Am. 87 (1990) 7120–7124.
[18] L. Eisoldt, A. Smith, T. Scheibel, Decoding the secrets of spider silk, Mater. Today. 14 (2011) 80–86, https://doi.org/10.1016/S1369-7021(11)70057-8.
[19] L. Römer, T. Scheibel, The elaborate structure of spider silk: structure and function of a natural high performance fiber, Prion 2 (2008) 154–161.
[20] P. Mohammadi, A.S. Aranko, L. Lemetti, Z. Cenev, Q. Zhou, S. Virtanen, C.P. Landowski, M. Penttilä, W.J. Fischer, W. Wagermaier, M.B. Linder, Phase transitions as intermediate steps in the formation of molecularly engineered protein fibers, Commun. Biol. 1 (2018) 86, https://doi.org/10.1038/s42003-018-0090-y.
[21] W. Wei, Y. Tan, N.R. Martinez Rodriguez, J. Yu, J.N. Israelachvili, J.H. Waite, A mussel-derived one component adhesive coacervate, Acta Biomater. 10 (2014) 1663–1670, https://doi.org/10.1016/j.actbio.2013.09.007.
[22] J. Tormo, R. Lamed, A.J. Chirino, E. Morag, E.A. Bayer, Y. Shoham, T.A. Steitz, structure of a bacterial family-III cellulose-binding domain: a general mechanism for attachment to cellulose, EMBO J. 15 (1996) 5739.
[23] P. Mohammadi, G. Beaune, B. Stokke, J.V.I. Timonen, M.B. Linder, Self-coacervation of a silk-like protein and its use as an adhesive for cellulosic materials, ACS Macro Lett. 7 (2018) 1120–1125.
[24] R. Hancock, A role for macromolecular crowding effects in the assembly and function of compartments in the nucleus, J. Struct. Biol. 146 (2004) 281–290, https://doi.org/10.1016/j.jsb.2003.12.008.
[25] R. Hancock, Self-association of polynucleosome chains by macromolecular crowding, Eur. Biophys. J. 37 (2008) 1059–1064, https://doi.org/10.1007/s00249-008-0276-1.
[26] M. Senske, L. Törk, B. Born, M. Havenith, C. Herrmann, S. Ebbinghaus, Protein stabilization by macromolecular crowding through enthalpy rather than entropy, J. Am. Chem. Soc. 136 (2014) 9036–9041, https://doi.org/10.1021/ja503205y.
[27] J. Ådén, P. Wittung-Stafshede, Folding of an unfolded protein by macromolecular crowding in vitro, Biochemistry. 53 (2014) 2271–2277, https://doi.org/10.1021/bi500222g.
[28] R. Hancock, K.W. Jeon, New Models of The Cell Nucleus: Crowding, Entropic Forces, Phase Separation, and Fractals, 2014.
[29] M.C. Konopka, I.A. Shkel, S. Cayley, M.T. Record, J.C. Weisshaar, Crowding and confinement effects on protein diffusion in vivo, J. Bacteriol. 188 (2006) 6115–6123, https://doi.org/10.1128/JB.01982-05.
[30] D. Huemmerich, C.W. Helsen, S. Quedzuweit, J. Oschmann, J. Oschmann, R. Rudolph, T. Scheibel, Primary structure elements of spider dragline silks and their contribution to protein solubility, Biochemistry. 43 (2004) 13604–13612 http://pubs.acs.org/doi/abs/10.1021/bi048983q.
[31] J.M. Gosline, P.a. Guerette, C.S. Ortlepp, K.N. Savage, The mechanical design of spider silks: from fibroin sequence to mechanical function, J. Exp. Biol. 202 (1999) 3295–3303.
[32] B. Demeler, A comprehensive data analysis software package for analytical ultracentrifugation experiments, Mod. Anal. Ultracentrifugation Tech. R. Soc. Chem. (2005) 210–229.
[33] H. Durchschlag, Specific volumes of biological macromolecules and some other molecules of biological inerest, in: H. Hinz (Ed.), Thermodyn. Data Biochem. Biotechnol. Springer, Berlin, 1986, pp. 45–128, , https://doi.org/10.1007/978-3-642-71114-5_3.
[34] E. Brookes, B. Demeler, Genetic algorithm optimization for obtaining accurate molecular weight distributions from sedimentation velocity experiments, Anal. Ultracentrifugation VIII. 131 (2006) 33–40.
[35] E.H. Brookes, B. Demeler, Parsimonious regularization using genetic algorithms applied to the analysis of analytical ultracentrifugation experiments, Proc. 9th Annu. Conf. Genet Evol. Comput. (2007) 361–368, https://doi.org/10.1145/1276958.1277035.
[36] D. Axelrod, D.E. Koppel, J. Schlessinger, E. Elson, W.W. Webb, Mobility measurement by analysis of fluorescence photobleaching recovery kinetics, Biophys. J. 16 (1976) 1055–1069.
[37] E. Nordmeier, Static and dynamic light-scattering solution behavior of pullulan and dextran in comparison, J. Phys. Chem. 97 (1993) 5770–5785, https://doi.org/10.1021/j100123a050.
[38] H.-X. Zhou, G. Rivas, A.P. Minton, Macromolecular crowding and confinement: biochemical, biophysical, and potential physiological consequences, Annu. Rev. Biophys. 37 (2008) 375–397, https://doi.org/10.1146/annurev.biophys.37.032807.125817.
[39] M.R. Kasaai, Dilute solution properties and degree of chain branching for dextran, Carbohydr. Polym. 88 (2012) 373–381, https://doi.org/10.1016/j.carbpol.2011.12.012.
[40] A.I. Leonov, A theory of necking in semi-crystalline polymers, Int. J. Solids Struct. 39 (2002) 5913–5926, https://doi.org/10.1016/S0020-7683(02)00478-X.
[41] A. Barth, Infrared spectroscopy of proteins, Biochim. Biophys. Acta - Bioenerg. 1767 (2007) 1073–1101, https://doi.org/10.1016/j.bbabio.2007.06.004.
[42] E. Morris, Frontiers in Carbohydrate Research: Food Applications, Elsevier Applied Science, London, 1989.
[43] R.D. McCurdy, H.D. Goff, D.W. Stanley, A.P. Stone, Rheological properties of dextran related to food applications, Food Hydrocoll. 8 (1994) 609–623.
[44] S.K. Ramadugu, Y. Chung, J. Xia, C.J. Margulis, When sugars get wet. A comprehensive study of the behavior of water on the surface of oligosaccharides, J. Phys. Chem. B. 113 (2009) 11003–11015.
[45] A.B. Kayitmazer, Thermodynamics of complex coacervation, Adv. Colloid Interf. Sci. 239 (2017) 169–177, https://doi.org/10.1016/j.cis.2016.07.006.
[46] J.C. Martinez, J. Murciano-Calles, E.S.M. Iglesias-Bexiga, I. Luque, J. Ruiz-Sanz, Isothermal Titration Calorimetry: Thermodynamic Analysis of the Binding Thermograms of Molecular Recognition Events by Using Equilibrium Models, Appl. Calorim. a Wide Context - Differ. Scanning Calorimetry, Isothermal Titration Calorim. Microcalorim. (2013) 73–104, https://doi.org/10.5772/53311.
[47] M. Nigen, T. Croguennec, D. Renard, S. Bouhallab, Temperature affects the supramolecular structures resulting from α-lactalbumin - Lysozyme interaction, Biochemistry 46 (2007) 1248–1255, https://doi.org/10.1021/bi062129c.
[48] J. Doublier, C. Garnier, D. Renarda, C. Sanchezb, Protein-polysaccharide interactions, Curr. Opin. Colloid Interf. Sci. 5 (2000) 202–214.